Journal of
Applied Crystallography

ISSN 0021-8898

Received 16 August 2006
Accepted 13 November 2006

© 2007 International Union of Crystallography
Printed in Great Britain – all rights reserved

Gibbs–Thomson analysis of crystalline poly(9,9-di-*n*-octyl-2,7-fluorene)

S. H. Chen,[a] C. H. Su,[b,c] A. C. Su,[b,d]* Y. S. Sun,[c] U. Jeng[c] and S. A. Chen[d]

[a]Department of Materials Science and Engineering, National Dong Hwa University, Hualien 974, Taiwan, [b]Institute of Materials Science and Engineering, National Sun Yat-sen University, Kaohsiung 804, Taiwan, [c]National Synchrotron Radiation Research Center, Hsinchu 300, Taiwan, and [d]Department of Chemical Engineering, National Tsing Hua University, Hsinchu 300, Taiwan. Correspondence e-mail: acsu@mx.nthu.edu.tw

Based on results of small-angle X-ray scattering and differential scanning calorimetric measurements, the equilibrium melting temperature and basal surface energy (σ_e) of crystalline poly(9,9-di-*n*-octyl-2,7-fluorene) (PFO) were preliminarily estimated as *ca* 451.6 K and 0.084 J m^{-2}, respectively, *via* Gibbs–Thomson analysis. This σ_e value leads to a value of 76 kJ mol^{-1} for the work of fold that greatly exceeds the values for typical polymers, reflecting the semi-rigid nature of the PFO backbone and consistent with the large-loop folds proposed earlier for this particular conjugated-backbone polymer. This is in strong contrast to the commonly held belief that conjugated polymers are generally too rigid to form folded-chain lamellar crystals.

1. Introduction

Using poly(9,9-di-*n*-octyl-2,7-fluorene) [PFO, one of the most studied 'fruit flies' of semiconducting polymers (Kraft *et al.*, 1998; Friend *et al.*, 1999)] as an example, we showed conclusively in a previous electron microscopy study that, in contrast to common belief, a conjugated polymer may indeed form single crystals of folded-chain lamellae (Chen *et al.*, 2004). We have further argued that, in view of the semi-rigid nature of the PFO backbone, the formation of single crystals is unlikely to follow the adjacent re-entry mode of regime I crystallization in the Hoffman–Lauritzen picture (Hoffman *et al.*, 1976); instead, crystallization of PFO appears to proceed through attachment and coalescence of nanograins (*ca* 10 to 20 nm in size, much smaller than the contour length of the PFO chains) of collapsed chains to the crystal-growth front. We have therefore conjectured that the folds must be inherently loose and loop-like to avoid excessive penalties from unfavorable conformations in tight folds (Chen *et al.*, 2004). It is therefore of interest to have an estimate of the basal plane surface energy (σ_e) involved in such a loose-loop case.

By means of differential scanning calorimetric (DSC) and small-angle X-ray scattering (SAXS) measurements, here we show that the melting behavior of PFO is reminiscent of typical semicrystalline polymers. In addition, results of a straightforward Gibbs–Thomson analysis indicate that the equilibrium melting temperature T_m^o = 451.6 K and σ_e = 0.084 J m^{-2}. The latter is only moderately higher than typical values for semicrystalline polymers, which reflects the semi-rigid nature of the PFO backbone on the one hand and, on the other hand, is consistent with the loose-loop (and nonadjacent re-entry) folds proposed earlier for this particular conjugated-backbone polymer.

2. Experimental

The characteristics of the PFO sample have been described previously (Chen *et al.*, 2004). Differential scanning calorimetric (DSC) measurements were made using a TA Q100 instrument routinely calibrated using indium and lead standards at a heating rate of 20 K min^{-1} and operated under a stream of nitrogen gas. The typical DSC sample size is *ca* 3 mg.

Small-angle X-ray scattering (SAXS) was used to characterize the crystalline lamellar morphology of PFO. Prior to SAXS characterization, all the samples (discs *ca* 6 mm in diameter and *ca* 0.4 mm in thickness) were crystallized at selected temperatures (T_c) in a high-temperature stage (Linkam THMS-600 connected to a TMS-91 temperature controller) under a protective nitrogen atmosphere for different periods of time (t_c = 1 to 12 h, after which the crystallization process had practically ended) at temperatures ranging from T_c = 397 to 417 K. Samples were always heated to T_{max} = 523 K for 1 min to erase previous thermal histories, followed by jumping to T_c for isothermal crystallization and subsequent quenching into ice water.

SAXS measurements were performed at the BL01B beamline of the National Synchrotron Radiation Research Center (NSRRC). The wavelength of the incident X-ray beam was λ = 0.1181 nm (10.5 keV). With a sample-to-detector distance of 1571.4 mm and a beamstop of 4 mm diameter, we collected SAXS data using a one-dimensional position-sensitive detector (PSD). All the SAXS data were corrected for sample transmission, background, and the detector sensitivity. The modulus of the scattering vector q [= $4\pi\sin(\theta/2)/\lambda$], defined by the scattering angle θ and the wavelength λ of the X-rays, was calibrated using silver behenate. More details of the SAXS setup and the instrument calibration may be found in an earlier report (Lai *et al.*, 2005).

To enhance the scattering intensity, a stack of four PFO discs with the same thermal history was used in the SAXS measurement. Further corrections for removing irrelevant scattering characteristics at the low-q and high-q extremes were subsequently made using the Porod law (Roe, 2000; Higgins & Benoit, 1994) and the Debye–Bueche equation (Higgins & Benoit, 1994), as described in detail elsewhere (Liao *et al.*, 2002) , before final presentation as Lorentz-corrected profiles (Higgins & Benoit, 1994; Liao *et al.*, 2002).

Table 1
Summary of SAXS and DSC results.

T_c (K)	397	399	402	404	406	408	411	413	415	417
t_c (h)	1	1.5	2	2.5	3	4	6	8	10	12
L (nm)	25.7	27.6	28.2	29.0	30.3	32.9	31.8	33.1	34.2	36.2
l_c (nm)	10.7	11.1	11.8	11.4	12.1	12.8	12.6	13.4	14.1	14.3
l_a (nm)	15.0	16.5	16.4	17.6	18.2	20.1	19.2	19.7	20.1	21.9
T_H (K)	431.0	431.3	431.4	431.3	432.2	431.5	430.9	431.1	431.6	432.0
T_L (K)	407.1	410.3	410.3	416.5	418.5	422.4	420.9	421.0	423.4	424.2
T_{onset} (K)	400.8	404.0	403.5	409.5	412.2	414.8	415.7	415.0	418.0	417.5
X_c (%)	41.4	40.3	41.7	39.2	39.9	38.9	39.6	40.6	41.3	39.5
Measured ΔH (J g^{-1})	32.2	30.7	30.3	26.9	27.5	29.1	28.5	34.3	25.9	28.0
ΔH_f (J g^{-1}) at 100% crystallinity	77.7	76.3	72.6	68.7	69.0	74.8	72.0	84.6	62.7	70.8
Average value of ΔH_f at 100% crystallinity: 73 (12) J g^{-1}										

3. Results

Given in Fig. 1(*a*) are representative SAXS profiles of isothermally crystallized PFO specimens after Lorentz correction. Measured scattering intensities are generally weak, as the electron density contrast is only modest. This is reflected in the noise level in Fig. 1(*a*). As shown in Fig. 1(*b*), noise was nevertheless smoothed out during construction of the normalized one-dimensional (1D) correlation function (Higgins & Benoit, 1994; Strobl, 1996)

$$\gamma_1(z) = \int_0^\infty I(q)q^2 \cos(qz)\,\mathrm{d}q \Big/ \int_0^\infty I(q)q^2\,\mathrm{d}q, \qquad (1)$$

which represents a statistically averaged low-resolution view of the two-phase lamellar structure. Table 1 summarizes the processing conditions and morphological characteristics determined graphically (Strobl, 1996) from $\gamma_1(z)$, including the long period (L), the crystalline lamellar thickness (l_c), the amorphous layer thickness (l_a) and the fractional crystallinity $X_c = l_c/L$.

Corresponding DSC traces of these PFO specimens are shown in Fig. 2(*a*). The glass transition is easily identifiable at $T_g \simeq 333$ K. In the high-temperature range, there exist generally two endotherms: the one marked as T_L (which is *ca* 7 to 14 K above T_c) is attributed to initial melting of crystallites formed at T_c, whereas the high-temperature endotherm at T_H near 433 K is attributed to final

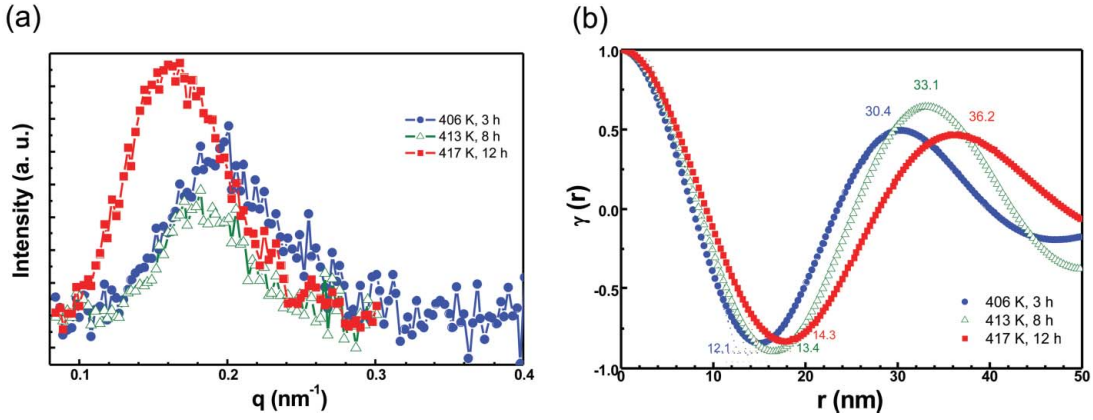

Figure 1
(*a*) Representative Lorentz-corrected and baseline-adjusted SAXS profiles of PFO specimens isothermally crystallized at different temperatures for different periods of time followed by quenching to room temperature. (*b*) Corresponding 1D correlation functions.

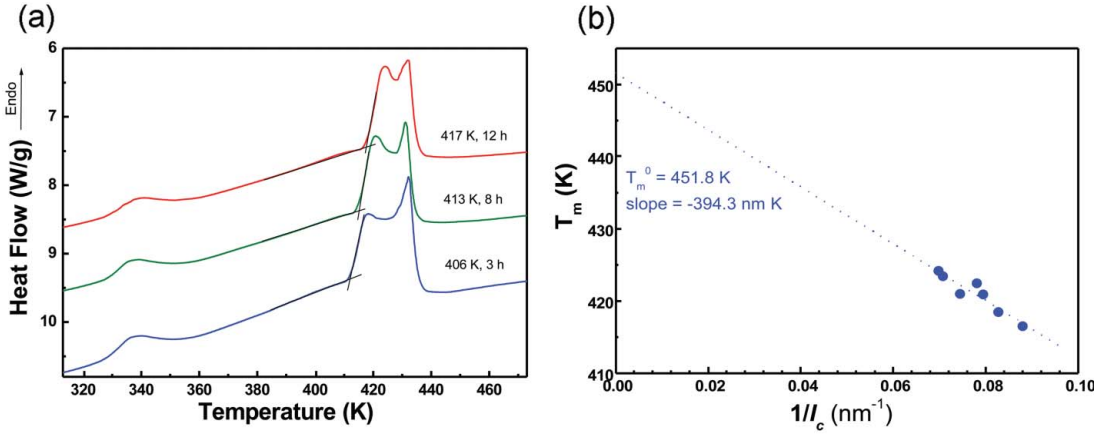

Figure 2
(*a*) Representative DSC traces of PFO specimens isothermally crystallized at different temperatures for different periods of time and subsequently quenched to room temperature. (*b*) Gibbs–Thomson plot of all ten specimens with T_{onset} taken as T_m.

melting of reorganized crystallites, as it is independent of T_c and is always located at the same position (Chen *et al.*, 2005) in spite of differences in crystallization conditions. To minimize errors arising from the effects of specimen superheating and melting-reorganization of crystallites during the DSC scan, we have operationally identified the melting temperature (T_m) with the onset (T_{onset}) of the low-temperature endotherm T_L. On the basis of the combined area (ΔH) under the endotherms and X_c determined from SAXS profiles, the heat of fusion ΔH_f for perfectly crystalline PFO is estimated as 73 (12) J g^{-1}. Values of these relevant parameters are also summarized in Table 1.

In terms of the Gibbs–Thomson model (Wunderlich, 1980), T_m of lamellar crystals depends on the crystalline lamellar thickness and the basal plane surface energy σ_e according to

$$T_m = T_m^o\left(1 - 2\sigma_e \big/ \rho l_c \Delta H_f\right), \qquad (2)$$

where ρ is the crystal density. A linear relationship is therefore expected when plotting T_m against l_c^{-1}, such as that given in Fig. 2(*b*) in the present case of PFO. From the values of the intercept and the slope, we find that T_m^o = 451.6 K and σ_e = 0.084 J m^{-2} with $\Delta H_f \simeq$ 73 J g^{-1} (Table 1) and theoretical density (Chen *et al.*, 2004) of 1.041 g ml^{-1}. In addition, from $\Delta H_f \simeq 73$ J g^{-1} = 29 kJ mol^{-1} and T_m^o = 452 K, one deduces that the entropy of fusion $\Delta S_f = \Delta H_f/T_m^o \simeq$ 64 J mol^{-1} K^{-1}.

4. Discussion

4.1. Comparison with σ_e of other polymers

Reported σ_e values for a given polymer are often notoriously scattered. Taking polyethylene (PE) as a representative example, σ_e values ranging from 0.04 to 0.10 J m^{-2} (*i.e.*, a span of ±40% on the basis of the mean value of 0.07 J m^{-2}) have been reported in the last four decades (Hocquet *et al.*, 2003). Many of the reported σ_e values were based on Lauritzen–Hoffman analysis of spherulitic growth rates (Hoffman *et al.*, 1976). In view of the large number of fitting parameters required in such an analysis, it is not really surprising that strong discrepancies exist in the σ_e values obtained for a given polymer by different groups of researchers. In our opinion, reliable values are those determined from the more rigorous Gibbs–Thomson approach. Limiting to the latter case would also facilitate more consistent comparison with present results of Gibbs–Thomson analysis on PFO. On the basis of such a criterion of data selection, one finds that σ_e = *ca* 0.06 J m^{-2} for PE (Hocquet *et al.*, 2003), syndiotactic polypropylene (Supaphol *et al.*, 2000), and poly(L-lactide) (Baratian *et al.*, 2001), *ca* 0.05 J m^{-2} for isotactic polypropylene (Yamada *et al.*, 2003), *ca* 0.03 J m^{-2} for poly(oxyethylene) (Schoenherr & Frank, 2003), and *ca* 0.02 J m^{-2} for the β phase of syndiotactic polystyrene (Wang *et al.*, 2002). It is clear that no consistent trend may be identified with chain rigidity. The present value of σ_e = 0.084 J m^{-2} for PFO indeed lies at the high end, but is only slightly higher than that of PE. As the fringed micelle model dictates strongly increased steric repulsion (Sperling, 2001) with lateral crystal size, this only moderately high value of σ_e implies that the fringed micelle model in its strict sense is unlikely to be applicable to PFO.

4.2. Comparison based on work of fold

For comparison with flexible polymers within the framework of tight folding in the adjacent re-entry model, a more meaningful parameter for comparison purposes would be the work of fold g instead of σ_e. Values of g typically lie within in the range 10 to 40 kJ mol^{-1}, increasing qualitatively with backbone rigidity from flexible polymers such as PE and polyethers to more rigid chains such as isotactic polystyrene and poly(*p*-phenylene sulfide) (Hoffman *et al.*, 1976). For the present case of PFO, we have g = 76 kJ mol^{-1} as calculated from the unit-cell dimensions a = 25.6 and b = 23.4 Å (Chen *et al.*, 2004). This value is way beyond the usual range of g values and certainly reflects the rigidity of PFO backbone. The issue, then, is whether this corresponds to large loops of folds as we proposed.

4.3. Folding of PFO chains

The polyfluorene backbone is not collinear, forming an angle of 160° between successive monomer units (Grell *et al.*, 1999). The shortest possible fold would then correspond to nine monomers (each 0.83 nm in length), spanning 5 nm across the basal plane. This corresponds to an average of 8.4 kJ mol^{-1} for a monomer in the loop for torsional displacements from the equilibrium chain conformation, which is a mild increase in energy and entirely possible to achieve as indicated by preliminary results of our molecular mechanics calculations.

To achieve efficient packing at the fold surface, however, these large loops must orient themselves in a particular direction to avoid steric conflicts. It is then gratifying to note that our morphological observations (Chen *et al.*, 2007) indeed show long {100} and short {110} facets (*i.e.*, sword-like) in micrometre-sized single crystals of PFO, reminiscent of growth habits of orthorhombic PE. Drawing an analogy to the case of PE, where chains are known to fold along the {110} plane, one is tempted to speculate that the fold plane in the case of PFO might also be {110}. In addition, these folds must have a pair of chains folding together to avoid steric conflicts for the eight-chain unit-cell structure (Chen *et al.*, 2004). The pairing (or embracing) action has been noted previously (Chen *et al.*, 2004). This type of paired folding would require a span of *ca* 1.74 nm to match the unit-cell dimensions, which is much shorter than that of the tight nine-monomer fold discussed above. It follows that more monomers are required to constitute such fold structure. Assuming a loop shape like the silhouette of an old-fashioned electric light bulb, we estimated that 21 monomers are needed. This brings the increase in torsional energy per monomer down further to *ca* 3.6 kJ mol^{-1}. As neighboring pairs along the {110} plane fold in opposite basal planes, the large bulb head, *ca* 5 nm in diameter, does not seem serious: allowing a slight distribution of loop heights would easily alleviate steric repulsion. Such a fold structure would corresponds to an amorphous region *ca* 7 nm in thickness and hence predicts a *minimum* value of l_a as *ca* 14 nm, consistent with our SAXS results in Table 1. The model is certainly only speculative at the present stage and awaits further confirmations.

The discussion above corresponds to the ideal limit of perfect folding. As in many polymer crystals grown from melt under large supercoolings, the random-switchboard model is likely to serve as a more realistic representation (Sperling, 2001). This means a thick amorphous layer on top of the fold plane, in agreement with the range of 15 to 22 nm observed here. Like general cases described by the random-switchboard model, one would also expect a high density of defects (Sperling, 2001) in PFO crystals; this is particularly likely in view of stronger steric complications resulting from the unusually large loop size of PFO folds. The short lifetime (several seconds, an order of magnitude lower than typical melt-grown polymer crystals) of diffraction patterns for polyfluorene crystals under an electron beam (Chen *et al.*, 2005, 2006) is therefore a natural consequence.

We gratefully acknowledge financial support from the Ministry of Education (Program for Promoting Academic Excellence of Universities, grant No. 91E-FA04-2-4A) and the National Science Council (grant No. NSC92-2216-E-110-009).

References

Baratian, S., Hall, E. S., Lin, J. S., Xu, R. & Runt, J. (2001). *Macromolecules*, **34**, 4857–4864.
Chen, S. H., Chou, H. L., Su, A. C. & Chen, S. A. (2004). *Macromolecules*, **37**, 6833–6838.
Chen, S. H., Su, A. C. & Chen, S. A. (2005). *J. Phys. Chem. B*, **109**, 10067–10072.
Chen, S. H., Su, A. C. & Chen, S. A. (2007). *Macromolecules*. In the press.
Chen, S. H., Su, A. C., Su, C. H. & Chen, S. A. (2006). *J. Phys. Chem. B*, **110**, 4007–4013.
Friend, R. H., Gymer, R. W., Holmes, A. B., Burroughes, J. H., Marks, R. N., Taliani, C., Bradley, D. D. C., dos Santos, D. A., Gredas, J. L., Loglund, M. & Salaneck, W. R. (1999). *Nature (London)*, **397**, 121–128.
Grell, M., Bradley, D. D. C., Ungar, G., Hill, J. & Whitehead, K. S. (1999). *Macromolecules*, **32**, 5810–5817.
Higgins, J. S. & Benoit, H.C. (1994). *Polymers and Neutron Scattering*. New York: Oxford University Press.
Hocquet, S., Dosiere, M., Thierry, A., Lotz, B., Koch, M. H. J., Dubreuil, N. & Ivanov, D. A. (2003). *Macromolecules*, **36**, 8376–8384.
Hoffman, J. D., Davis, G. T. & Lauritzen, J. I. (1976). *Treatise in Solid State Chemistry*, edited by N. B. Hannay. New York: Plenum.
Kraft, A., Grimsdale, A. C. & Holmes, A. B. (1998). *Angew. Chem. Int. Ed. Engl.* **37**, 402–428.
Lai, Y. H., Sun, Y. S., Jeng, U., Song, Y. F., Tsang, K. L. & Liang, K. S. (2005). *Nucl. Instrum. Methods Phys. Res. B*, **238**, 205–213.
Liao, W. P., Lin, T. L., Woo, E. M. & Wang, C. (2002). *J. Polym. Res.* **9**, 91–96.
Roe, R. J. (2000). *Methods of X-ray and Neutron Scattering in Polymer Science*. Oxford University Press.
Schoenherr, H. & Frank, C. W. (2003). *Macromolecules*, **36**, 1199–1208.
Sperling, L. H. (2001). *Introduction to Physical Polymer Science*, 3rd ed., ch. 6. New York: Wiley.
Strobl, G. (1996). *The Physics of Polymers*. Berlin: Springer.
Supaphol, P., Spruiell, J. E. & Lin, J. S. (2000). *Polym. Int.* **49**, 1473–1482.
Wang, C., Cheng, Y. W., Hsu, Y. C. & Lin, T. L. (2002). *J. Polym. Sci. Polym. Phys.* **40**, 1626–1636.
Wunderlich, B. (1980). *Macromolecular Physics*, Vol. 3, ch. 8. New York: Academic Press.
Yamada, K., Hikosaka, M., Toda, A., Yamazaki, S. & Tagashira, K. (2003). *J. Macromol. Sci.* **B42**, 733–752.